Alkynyl gold(I) complex triggers necroptosis via ROS generation in colorectal carcinoma cells

Inés Mármol, María Virumbrales-Muñoz, Javier Quero, Cristina Sánchez-de-Diego, Luis Fernández, Ignacio Ochoa, Elena Cerrada, Mª. Jesús Rodríguez Yoldi

PII: S0162-0134(17)30413-0
DOI: doi: 10.1016/j.jinorgbio.2017.08.020

Alkynyl gold(I) complex triggers necroptosis via ROS generation in colorectal carcinoma cells

Inés Mármol[a], María Virumbrales-Muñoz[b], Javier Quero[a], Cristina Sánchez-de-Diego[c], Luis Fernández[b], Ignacio Ochoa[b], Elena Cerrada[d,] and M[a] Jesús Rodríguez Yoldi[a,*]*

[a]*Department of Pharmacology and Physiology, University of Zaragoza, Zaragoza, Spain, CIBERobn, IIS Aragón, IA2.*

[b]*Group of Applied Mechanics and Bioengineering (AMB). University of Zaragoza, Zaragoza, Spain, CIBER-BBN, I3A, Aragon Institute of Biomedical Research.*

[c]*Departament of Physiological Sciences II, University of Barcelona, Barcelona, Spain.*

[d]*Department of Inorganic Chemistry, University of Zaragoza, Zaragoza, Spain, ISQCH-C.S.I.C.*

Abstract: Given the rise of apoptosis-resistant tumors, exists a growing interest in developing new drugs capable of inducing different types of cell death

to reduce colorectal cancer-related death rates. As apoptosis and necroptosis do not share cellular machinery, necroptosis induction may have a great therapeutic potential on those apoptosis-resistant cancers, despite the inflammatory effects associated with it. We have synthesized an alkynyl gold(I) complex [Au(C≡C-2-NC_5H_4)(PTA)] whose anticancer effect was tested on the colorectal adenocarcinoma Caco-2 cell line. With regard to its mechanism of action, this gold complex enters the mitochondria and disrupts its normal function, leading to an increase in ROS production, which triggers necroptosis. Necroptosis induction has been found dependent of TNF-α and TNFR1 binding, RIP1 activation and NF-κB signaling. Moreover, the antitumor potential of [Au(C≡C-2-NC_5H_4)(PTA)] has also been confirmed on the 3D cancer model spheroid. Overall, the obtained data show firstly that gold complexes might have the ability of inducing necroptosis, and secondarily that our compound [Au(C≡C-2-NC_5H_4)(PTA)] is an interesting alternative to current chemotherapy drugs in cases of apoptosis resistance.

KEYWORDS Gold complex, cancer, necroptosis, ROS, Caco-2 cells

INTRODUCTION

The use of metals with therapeutic purposes dates back to ancient times. Nevertheless one of the biggest successes for inorganic chemistry in medicine was the accidental discovery of antitumor properties of *cisplatin* in the 60s. *cis*-[$PtCl_2(NH_3)_2$], commonly called *cisplatin* has been used worldwide in chemotherapy against various cancers including testicular, ovarian and solid tumors of head and neck [1,2]. However, the use of platinum derivatives results in serious side effects related to their nonspecific mechanism of action [3]. Thus, in the last decades researchers have focused on finding new metal derivatives with anticancer properties that lack the shortcomings of *cisplatin* and its analogues.

In this context, gold complexes are an interesting alternative to platinum-containing drugs [1,2]. Many gold(I) complexes have been tested against various tumor cell lines, [4-6] and some of these promising *in vitro* results have also been confirmed *in vivo* using animal models [4,7,8]. The main advantage of these compounds against platinum complexes is that they differ in their mechanism of action. Whereas platinum compounds interact with nucleic acids, gold-containing drugs display a higher variety of targets, including non-canonical DNA structures [9, 10], zinc finger proteins [11] or the redox enzyme thioredoxin reductase (TrxR). Gold complexes are able to inhibit TrxR via interacting with the selenium atom [12] of the selenocysteine moiety. When TrxR is inhibited, the regular redox balance becomes disrupted and the abnormally increased levels of reactive oxygen species (ROS) trigger cell death [13]. Consequently, TrxR inhibition does not involve the side effects related to treatment with *cisplatin* and its analogues. In addition, there is not cross-resistance between them [14]. Therefore, gold-containing drugs are able to induce cell death even in *cisplatin*-resistant cancer cells.

Colorectal cancer (CRC) is one of the most prevalent cancers in Western countries and one of the main causes of cancer-related death [15]. CRC is a kind of tumors which shows a good response to treatment with metallic compounds, since the combination of the *cisplatin* analogue *oxaliplatin* (*cis*-[oxalate(*trans*-*l*-1,2-diaminocyclohexane)platinum(II)]) and traditional chemotherapy improves patient response versus traditional chemotherapy alone [16,17]. Consequently, it is necessary to

find new therapeutic options with fewer side effects than current treatments but maintaining their anticancer potential.

Treatment with metallic compounds usually induces apoptosis, one of the best characterized kinds of cell death [18, 19]. As an example, we have recently described in detail the apoptotic insights of an alkynyl gold(I) complex [20]. But, given the rise of apoptosis-resistant tumors exist a growing interest in developing new drugs capable of inducing different types of cell death [21].

Necroptosis is a regulated form of necrosis mainly governed by Receptor-Interacting Protein 1 (RIP1), RIP3 and Mixed Lineage Kinase Domain-Like (MLKL) protein. A wide range of stimuli can start this process, although the best studied pathway is triggered by Tumor Necrosis Factor (TNF). TNF-triggered necroptosis requires the formation of "necrosome", a protein complex in which RIP1 and RIP3 are involved and responsible for MLKL phosphorylation. The necrosome migrates to plasma membrane and induces its rupture, [22, 23] so it is the ultimate responsible for necroptotic morphological features, *i.e.* cellular swelling and loss of intracellular content. Therefore, as apoptosis and necroptosis do not share the same molecular pathways, necroptosis-inducing drugs may induce cell death on apoptosis-resistant tumors.

2D cell culture provides only a slanted vision of how cells behave inside human body; therefore, results in 2D cannot always be translated into *in vivo* settings. To obtain more accurate information about cell response to that observed *in vivo*, 3D cell cultures have proved an useful alternative [24]. 3D cell models provide a more relevant microenvironment where cell-cell and cell-matrix interactions are promoted. Particularly, cells acquire relevant features observed in tumors *in vivo*, such as distinctive morphological and cellular characteristics, as well as distinctive gene expression signature, which could account for the different drug response to that observed in 2D [25, 26]. Among the 3D cell culture methods, spheroids are one of the best characterized models so far. They closely recapitulate the tumor microenvironment, including hypoxia and metabolic gradients. Furthermore, previous studies in spheroids have provided insight on drug distribution and penetration. [27, 28]. All in all, cell spheroids are a 3D cell culture method usually used in drug-response studies [29, 30]. Specifically, Caco-2 spheroids have been previously used in permeability assays as the obtained values were quite similar to those found *in vivo* [31].

Here we describe the preparation and evaluation of the anticancer activity of the alkynyl gold(I) derivative [Au(C≡C-2-NC_5H_4)(PTA)] (~~Chart~~ Scheme 1) against human colon cancer cells (Caco-2). We have established its ability to induce necroptosis by increasing ROS levels, which triggers cell death. Due to the spontaneous differentiation of Caco-2 cells to normal enterocytes after 15 days growing [32], we were able to compare its effect on both CRC and healthy tissue. Additionally, data obtained in 2D cell model were expanded by testing the antiproliferative effect of the compound on 3D spheroid model.

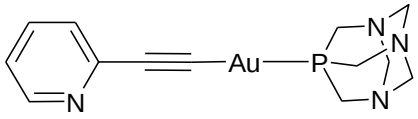

Scheme 1. Chemical structure of [Au(C≡C-2-NC_5H_4)(PTA)].

MATERIALS AND METHODS

Preparation of [Au(C≡C-2-NC_5H_4)(PTA)]. The alkynyl gold complex was prepared as described previously by some of us [33]. Pale yellow solid was isolated in 78% yield. ^{1}H NMR (400 MHz, $CDCl_3$, 25 °C): δ = 4.37 and 4.51 (AB system, 6H, NCH_2N), 4.33 (s, 6H, NCH_2P), 7.01 (dd, J = 4.8/1.5Hz, 1H, NC_5H_4 (H^5)), 7.3 (d J = 7.8, NC_5H_4 (H^3)), 7.48 (td, J = 7.6/1.5Hz, 1H, NC_5H_4 (H^4)), 8.42 (d, J = 4.8Hz, 1H, NC_5H_4 (H^6)) ppm. ^{31}P{^{1}H} NMR (162 MHz, $CDCl_3$, 25 °C): δ = –51.8 ppm. ^{13}C{^{1}H} NMR (75.4 MHz, $CDCl_3$, 25 °C): δ = 51.1 (d, J = 16 Hz, NCH_2P), 68.4 (s, Au*C*≡C), 72.2 (s, NCH_2N), 85.1 (s, AuC≡*C*), 121.8 (s, $C^{5,3}$-Py), 130,7 (s, C^4-Py), 150.3 (s, C^6-Py). IR (KBr): 2105 cm^{-1} ν(C≡C). FAB MS: *m/z* = 457 [M]$^+$. Elemental analysis calcd. (%) for $C_{13}H_{16}AuN_4P$ (456.23): C 34.22, H 3.53, N 12.28; found: C 34.55, H 3.75, N 12.50.

Chemical stability. The stability of the gold complex was analyzed by absorption UV spectroscopy. UV-Vis absorption spectra were recorded on a Thermo Scientific spectrophotometer. 10 mM solution of [Au(C≡C-2-NC_5H_4)(PTA)] in DMSO was diluted in 10^{-4} M PBS pH = 7.4 and thereafter monitored by measuring the electronic spectra over 24 h at 37°C. Additionally, a phosphate-buffered saline solution, pH 7.4 was added to a d_6-DMSO solution of the complex in a proportion 1:1 (due to the low solubility in water solution) and studied by NMR over 24h period.

Distribution coefficient ($logD_{7.4}$). The n-octanol-water partition coefficient of [Au(C≡C-2-NC_5H_4)(PTA)] was determined as previously reported using a shake-flask method [33]. The concentration of the compound in each phase was determined using UV absorbance spectroscopy. Log$D_{7.4}$ was defined as log{[$compound_{(organic)}$]/[$compound_{(aqueous)}$]}.

Interaction with BSA. Interaction of gold complex and bovine serum albumin (purchased from Sigma Aldrich) was analyzed as previously described by some of us [20].

DNA binding studies. Interaction of gold complex with DNA was studied using 3 nM pIRES2-EGFP plasmid (Clontech). Gold complex was diluted in miliQ water and different ratio of gold complex toplasmid were incubated 24 h at 37ºC. Electrophoretic mobility shift assays were performed by PAGE electrophoresis (90 min, 50 V) in TBE buffer using SYBR Safe as stain.

Cell culture. Human Caco-2 cell line (TC7 clone) was kindly provided by Dr. Edith Brot-Laroche (Université Pierre et Marie Curie-Paris 6, UMR S 872, Les Cordeliers, France). Caco-2 cells were maintained in a humidified atmosphere of 5% CO_2 at 37ºC. Cells (passages 50-80) were grown in Dulbecco's Modified Eagles medium (DMEM) (Gibco Invitrogen, Paisley, UK) supplemented with 20% fetal bovine serum (FBS), 1% non-essential amino acids, 1% penicillin (1000 U/mL), 1% streptomycin (1000 µg/mL) and 1% amphoterycin (250 U/mL). The cells were passaged enzymatically with 0.25% trypsin-1 mM EDTA and sub-cultured on 25 or 75 cm^2 plastic flasks at a density of $2 \cdot 10^4$ cells/cm^2. Culture medium was replaced every 2 days. Cell confluence (80%) - considered as differentiated cells- was confirmed by microscopic observance. Experiments in undifferentiated cells were performed 24 hours post-seeding.

Human MCF-7 cell line was kindly provided by Dr. Carlos J. Ciudad y Dra. Verònica Noé (Departamento de Bioquímica y Fisiología, Facultad de Farmacia, Universidad de Barcelona, Spain). MCF-7 cells were maintained in the same conditions as described for Caco-2 cell line.

Cell proliferation assay and IC_{50} value determination. Cell proliferation inhibition was measured using the MTT assay [34]. Caco-2/TC7 cells were plated in 96-well plates at a density of 4000 cells/well and incubated for 24 h under standard cell culture conditions. For IC_{50} values determination, a stock solution of the gold complex in

dimethyl sulfoxide (DMSO) was added to cells in a concentration range of 0-20 μM (10 replicates, 100 μL per well); cells treated with the same amount DMSO were used as negative control. Cells were exposed to the gold complex for 24 h and then 10 μL of MTT (5 mg/ml) was added. Incubation was continued at 37ºC for 3 h. Medium was then removed by inversion and 100 μL of DMSO/well were added. Absorbance at 560 nm - proportional to number of live cells- was measured by spectrophotometry (DTX 800, Beckman Coulter) and converted into percentage of growth inhibition.

Thioredoxin reductase activity assay in cells. Caco-2/TC7 were grown in 96-well plate at a density of 4.000 cells/well during 24h, and then treated with [Au(C≡C-2-NC_5H_4)(PTA)] for 24 h. After the incubation, cells were lysed with lysis buffer (50 mM Tris-HCl pH 7.5, 2 mM EDTA, protease inhibitor cocktail and distilled H_2O) for 30 min at room temperature. Then, TrxR inhibitor was added to each well and incubated 30 min. Cell lysates were incubated with reaction buffer (PBS pH 7, 100 mM EDTA, 0.05% BSA, 20 mM NADPH, distilled H_2O) with or without TrxR inhibitor. Reaction was started by adding 25 μL of 5,5-dithio-bis-(2-nitrobenzoic acid) (DTNB, 20mM in pure ethanol). Absorbance at 405nm was recorded every 10s for 6min as a measurement of thioredoxin reductase activity. TrxR activity was normalized by the amount of protein present in each well, determined by Bradford method.

Glutathione activity assay in cells. Caco-2/TC7 were grown in 96-well plate at a density of 4.000 cells/well during 24h, and then treated with [Au(C≡C-2-NC_5H_4)(PTA)] for 24 h. After the incubation, cells were lysed with modified RIPA buffer (50 mM Tris-HCl, 50 mM NaCl, 1 mM EDTA, 1% Triton X-100, 1% SDS, 1% DOC, 1 mM NaF, in miliQ water) with proteases inhibitors. Cell solution was shaken at RT for 20min, centrifuged for 5 min at 1200 rpm and resuspended in PBS. Then, reaction solution was added (0.1 M Tris-HCl pH 8.1, 0.02 mM NADPH, in PBS). Finally, reaction was started by adding 0.52 mM GSSG. Absorbance at 3340 nm was recorded for 6 min. Glutathione reductase activity of the cell lysate was measured as a loss in absorbance at 340 nm.

Measurements of apoptosis. Caco-2/TC7 cells were exposed to IC_{50} of [Au(C≡C-2-NC_5H_4)(PTA)] for 24 h, then collected and stained with Annexin V-FITC as described by Sánchez-de-Diego *et al* [20]. Untreated cells were used as negative control, in order to define basal levels of apoptosis, necrosis and cell death.

Propidium iodide staining of DNA content and cell cycle analysis. Caco-2/TC7 cells were exposed to IC_{50} of [Au(C≡C-2-NC_5H_4)(PTA)] for 24 h and then DNA content was analyzed as described by Sánchez-de-Diego *et al* [20].

Caspase activity studies. Caspase activation was studied using *CellEvent™ Caspase-3/7detection reagent* (C10423, ThermoFisher). Caco-2/TC7 cells were plated in 96-well plates at a density of 4000 cells per well and incubated for 24 h under standard cell culture conditions. For treatment, IC_{50} of [Au(C≡C-2-NC_5H_4)(PTA)] was added to cells and incubated 24 h; mock-treated cells were incubated with DMSO. Then, medium was removed and the reagent, previously diluted in PBS (90 µL /mL), was added to the cells. After 10 min of incubation, fluorescence was observed using confocal microscopy in a Nikon Eclipse Ti® inverted fluorescence microscope, coupled with a confocal module. Excitation and emission settings were 488 and 590/50 nm respectively. The intensity of fluorescence was analyzed with Fiji software (http://fiji.sc/Fiji).

Measurement of total cellular oxidative stress. Caco-2/TC7 cells were exposed to IC_{50} of [Au(C≡C-2-NC_5H_4)(PTA)] for 80 min and then *CellROX® Deep Red Reagent* (C10422, ThermoFisher) was added to a final concentration of 5 µM. Cells were incubated 30 min at 37ºC. Fluorescence was analyzed using confocal microscopy in a Nikon Eclipse Ti® inverted fluorescence microscope, coupled with a confocal module. Excitation and emission settings were 644 and 665 nm, respectively. The intensity of fluorescence was analyzed with Fiji software (http://fiji.sc/Fiji) and is considered a reflection of total intracellular ROS.

Determination of H_2O_2 cellular levels. H_2O_2 production was assessed using the dichlorofluorescein (DCF) assay [35]. Caco-2/TC7 cells were plated in 96-well plates at a density of 4000 cells per well and incubated for 24 h under standard cell culture conditions. For treatment, IC_{50} of [Au(C≡C-2-NC_5H_4)(PTA)] was added to cells and incubated 80 min; mock-treated cells were incubated with DMSO. Determination of H_2O_2 cellular levels was performed as described by Sánchez-de-Diego *et al.* [20].

Flow cytometry mitochondrial membrane potential assay. Caco-2/TC7 cells were plated in 75 cm^2 flasks at a density of 500.000 cells per flask and incubated 24 h under standard cell culture conditions. For treatment, IC_{50} of gold complex was added to each flask and incubated 24 h; mock-treated cells were incubated with DMSO. After treatment, changes in $\Delta\psi_m$ were analyzed as described by Sánchez-de-Diego *et al* [20].

Determination of RIP1 by flow cytometry. Caco-2/TC7 cells were plated in 75 cm^2 flasks at a density of 500.000 cells per flask and incubated 24 h under standard cell culture conditions. For treatment, IC_{50} of gold complex was added to each flask and incubated 24 h; mock-treated cells were incubated with DMSO. After treatment, cells were harvested and 100 µL of fixation solution INTRACELL (Intra 100-T, Immunostep) were added to each 50 µL of cells. Mix was incubated 5 min at room temperature and then was washed with PBS. Cells were resuspended in 50 µL PBS and 100 µL of permeabilisation solution INTRACELL (Intra 100-T, Immunostep) and 3 µL anti-RIP-1 antibody (Abcam ab72139, 1/100 dilution) were added. After 1 h incubation at 4ºC, cells were washed with 1 mL PBS and 50 µL of permeabilisation solution INTRACELL (Intra 100-T, Immunostep) were added. Finally, secondary antibody goat anti-mouse ALEXA 488 was added and samples were incubated 30 min at 4ºC. Cells were washed and resuspended in 200 µL PBS and fluorescence was analyzed by flow cytometry using a FACSARRAY BD equipped with an argon ion laser.

Caco-2 spheroids generation. Caco-2 cells ($3 \cdot 10^3$ cells per plate) were mixed with a high viscosity methylcellulose solution as described by Ayuso *et al* [36] and 100 µL of the final suspension were seeded on a round bottom 96-well plate. Spheroids were grown for 72 h and were then incubated with rising concentrations of [Au(C≡C-2-NC_5H_4)(PTA)] (3, 4 and 5 µM) for 24 h. For cell viability studies, spheroids were stained with Hoechst 33342 (4 mg/mL) and PI (4 mg/mL) for 30 min. Then, confocal microscopy images were taken as previously described.

RESULTS AND DISCUSSION

Solution chemistry. The alkynyl derivative [Au(C≡C-2-NC_5H_4)(PTA)] (**1**) was isolated as an stable light yellow solid in high yield. Its behavior in solution was analyzed by absorption spectroscopy and NMR. A phosphate-buffered saline (PBS) solution of the complex was incubated at 37ºC and studied by UV-visible spectroscopy over 24h. The

spectrum displays two intense bands around 215 and 290 nm and another band with lower intensity at 250 nm, attributed to electronic transitions from the alkyne ligand to the gold(I) center (Figure S2). These bands decrease their intensity over the time and a slight blue shift of the band at 290 nm is observed after 5h of incubation. Non-additional bands were observed during the experiment course and, more importantly, no new bands in the region of 500 nm, characteristic of colloidal gold(0) were detected. In addition, the NMR spectra in a mixture of PBS and d_6-DMSO solution revealed no decomposition and no release of the phosphane after 24h period (Figure S3). With these results, this complex can be considered sufficiently stable in the solution to be tested on cells.

The lipophilicity of a compound is associated to its diffusion and penetration into the cell membrane. Consequently, drug lipophilicity affects its activity, toxicity to healthy tissues and is directly related to plasma protein binding and metabolism of the drug [37]. Changes in drug lipophilicity by incorporating the suitable functional groups in the molecule have shown great impact in anticancer activity and host toxicity [38, 39]. However, phosphane gold(I) derivatives with high lipophilicity [39] tend to accumulate into mitochondria with the consequent serious effects [40]. Subsequently, a balanced relationship between lipophilicity and hydrophilicity would be highly desirable. Lipophilicity can be measured by the partition coefficient water/octanol, log$D_{7.4}$, which finally shows the corresponding balance between lipophilicity and hydrophilicity. The measurement of log$D_{7.4}$ of our alkynyl derivative (see experimental for details) gave a negative value next to 0 (-0.10). This is in accordance with slight hydrophilic character of the complex, albeit with a balanced relationship between both characters.

Binding to BSA. The distribution, free concentration and metabolism of a drug are affected by drug-protein interactions in the bloodstream [41, 42]. Such interaction can influence drug stability and toxicity during chemotherapeutic treatment, thereafter limiting drug efficacy. Consequently, it is important to understand the potential presence and nature of these interactions. One of the blood plasma proteins involved in drug transport is serum albumin. Bovine serum albumin (BSA) is frequently used in biochemical analysis due to its higher stability and accessibility. BSA contains two tryptophan residues (Trp-134 and Trp-212) in the former while HAS (human serum albumin) has a unique tryptophan. Hence, we have studied the interaction of [Au(C≡C-

2-NC_5H_4)(PTA)] with BSA by means of the measurement of the quenching of the intrinsic fluorescence of the amino acid tryptophan, which is sensitive to its local environment. Accordingly, any changes in the fluorescence emission spectra can be attributable to changes in the conformation, due to the presence of the quencher [43].

The fluorescence spectra of BSA were recorded in the presence of increasing amounts of the gold complex in the range of 310-450nm upon excitation at 295 nm. Quenching of the fluorescence is observed in a concentration dependent manner, without changes in the emission maximum and shape of the peaks (Figure 1A). This fact points to an interaction of the gold complex with the protein without alteration of the vicinity of the tryptophan residues.

The quenching process can be due to the presence of collisions between a fluorophore with the quenching agent -dynamic quenching- or the formation of a non-fluorescent complex with the quenching agent, *i.e.* static quenching. Fluorescence data were analyzed by the Stern-Volmer equation: $F_0/F = 1+ K_{sv}[\mathbf{1}]$, where F_0 and F are the steady sate fluorescence intensities of BSA before and after the addition of the gold complex. While a linear Stern-Volmer plot (F_0/F *vs.* [quencher]) is indicative of the occurrence of a single quenching mechanism, the plot F_0/F *vs* with a positive deviation (Figure 1B) suggests the presence of a combination or static and dynamic quenching. Moreover, the upward curvature in the plot indicates that both tryptophan residues in the BSA molecule are exposed to the gold complex [44].

The modified Stern-Volmer equation: $og\frac{(Fo-F)}{F} = \log Kb + n\ og[Q]$ provides the corresponding binding constant K_b, by using the plot of $\log(F_0\text{-}F)/F$ *vs* $\log[\mathbf{1}]$, (Figure 1C). The binding constant was found to be $2.3\cdot10^8$ M^{-1}, which indicates a high affinity of our complex to the protein, and inversely decreases with the temperature. This high value points to a strong interaction between BSA and the gold complex. The value of K_b of $2.46\cdot10^8$ increased four orders of magnitude in comparison to the related complex, with a phenyl ring instead of the pyridine molecule [Au(C≡C-C_5H_4)(PTA)] (K_b of $7.2\cdot10^4$ M^{-1})[41]. In order to calculate the nature of the binding sites between [Au(C≡C-2-NC_5H_4)(PTA)] and BSA, we have performed the quenching experiment at different temperatures (295, 304 and 310K). Values of n next to 2 indicate that there is more than one class of binding site in the interaction of the gold complex towards BSA.

Considering that we performed the quenching study at three temperatures, we can only approximate the corresponding thermodynamic parameters ΔH^o, ΔS^o and ΔG^o, which have been calculated from the equation $\ln K = -\Delta H^o/(RT) + \Delta S^o/R$, where K is the equilibrium constant at the three different temperatures, ΔH^o and ΔS^o are the standard enthalpy and entropy change for the reaction, respectively and R, the gas constant 8.314 $J \cdot mol^{-1}K^{-1}$. The calculated values for the experiment ΔH^o and ΔS^o provide $\Delta G^o < 0$ (Table 1, Figure S8)).

The interaction forces of biomolecules and drugs involve hydrophobic forces, electrostatic interactions, van der Waals interactions or hydrogen bonds [45]. The negative value calculated for ΔG^o is indicative of a spontaneous process and the negative values for both enthalpy and entropy of the interaction are consistent with the presence of van der Waals interaction and hydrogen bonds [45].

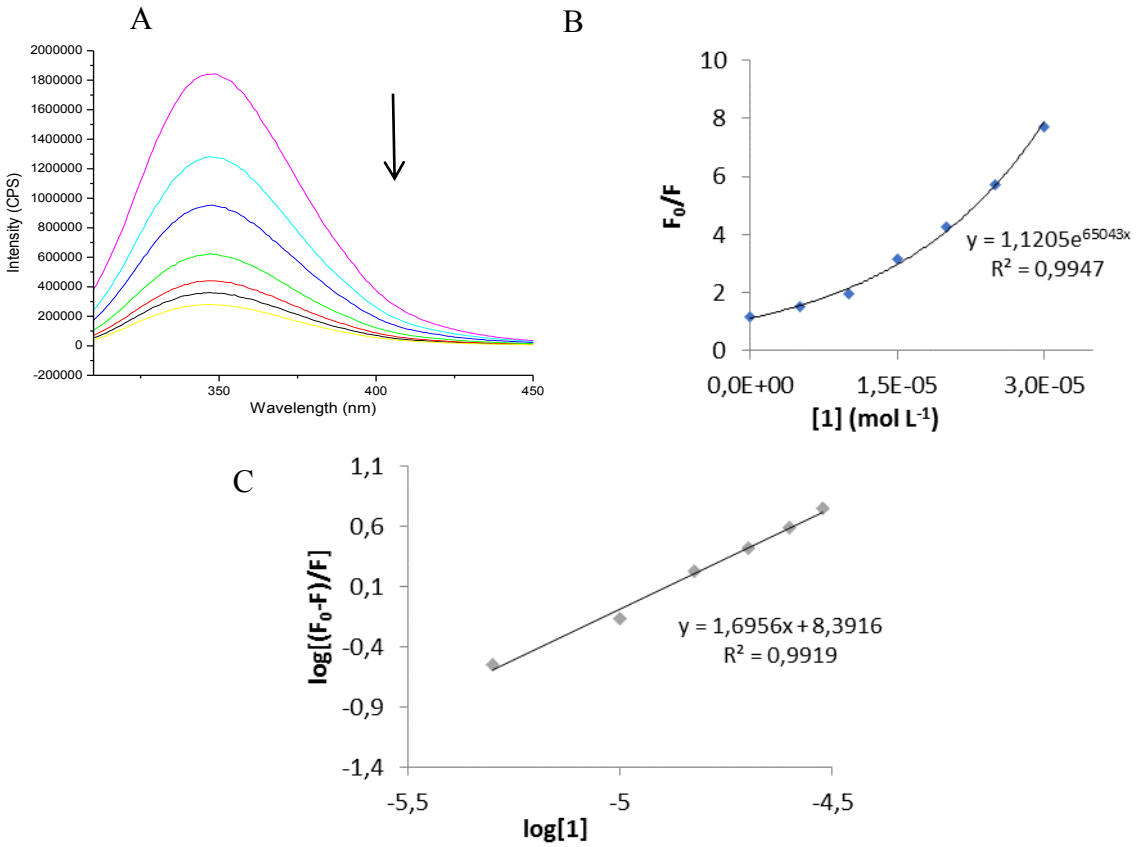

Figure 1. A) Fluorescence quenching of BSA in presence of increasing concentrations of [Au(C≡C-2-NC_5H_4)(PTA)] (**1**) at 295 K. Arrow indicates the increase of the quencher concentration. B) Stern-Volmer plot for the quenching of BSA with **1** at 295K. Stern-Volmer equation used: $F_0/F = 1 + K_{sv}[\mathbf{1}]$. C) Stern-Volmer equation used: $\log\{(F_0-F)/F\} = \log K_b + n\log[\mathbf{1}]$. The intercept of the best fit linear trend provides the Stern-Volmer quenching constant K_b.

Table 1. Thermodynamic parameters of [Au(C≡C-2-NC_5H_4)(PTA)]-BSA interaction.

T (K)	K_b (M^{-1})	n	ΔH^o (kJ·mol^{-1})	ΔS^o (J·mol^{-1}K^{-1})	ΔG^o (kJ·mol^{-1})
295	$2.46\cdot10^8$	1.70	-78.78	-105.9	-47.54
304	$8.98\cdot10^7$	1.62			-46.58
310	$5.95\cdot10^7$	1.60			-45.95

In addition, we have measured the UV-visible absorption spectra of the BSA in presence and in absence of the gold complex (figure S13). The absorption spectrum of

protein is only influences by complexation with quencher in ground state (static process). In our case a hyperchromism is observed after addition of the complex, which is in accordance with alteration in the microenvironment around the aromatic acid residues, whereas the presence of hypochromism is associated to an induced perturbation of α-helix of the protein with the quencher [46].

[Au(C≡C-2-NC_5H_4)(PTA)] antiproliferative activity. The *in vitro* effects of [Au(C≡C-2-NC_5H_4)(PTA)] toward human colon (Caco-2/TC7) and breast cancer (MCF-7) cell lines were tested using the colorimetric MTT assay. Firstly, we obtained the IC_{50} value after exposing cells to increasing drug amounts for 72 h (Table 2). Caco-2 cell line typically undergo enterocyte-like differentiation after reaching confluence, becoming polarized cell that expresses apical and basolateral surfaces with well-established tight junctions [30]. Consequently, it is possible to test the selectivity of the gold complex by testing its effects on differentiated cells (non-carcinogenic) in terms of viability. Undifferentiated Caco-2/TC7 cells showed higher sensibility to treatment compared with human breast cancer MCF-7 cells, with an IC_{50} value of 5-fold lower. These results suggest that therapeutic effect of [Au(C≡C-2-NC_5H_4)(PTA)] may be selective to colorectal cancer. On the other hand, [Au(C≡C-2-NC_5H_4)(PTA)] displayed a higher IC_{50} -up to 13-fold- on differentiated Caco-2 cells compared to the previously obtained on undifferentiated cells. Therefore, our compound might be selective to cancer tissue.

Finally, some of us have previously evaluated the antiproliferative effect of the reference drug cisplatin in Caco-2 cell line, obtaining an IC_{50} value of 45.6 ± 8.08 μM [47]. In conclusion, [Au(C≡C-2-NC_5H_4)(PTA)] shows higher cytotoxicity than cisplatin.

Table 2. Antiproliferative IC_{50} values of [Au(C≡C-2-NC_5H_4)(PTA)].

Cell line	IC_{50} value
Differentiated Caco-2/TC7	51.04± 1.28 µM
Undifferentiated Caco-2/TC7	3.8 ± 1.1 µM
MCF-7	19.02 ± 0.02 µM

In addition, further assays revealed that [Au(C≡C-2-NC_5H_4)(PTA)] antiproliferative effects on Caco-2 increased in a dose and time-dependent manner (Figure 2).

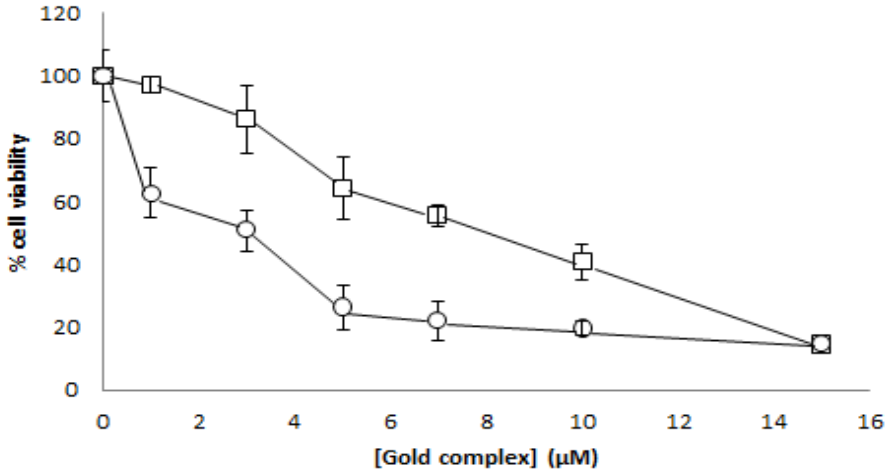

Figure 2. Survival curves of Caco-2 cells treated with increasing concentrations of [Au(C≡C-2-NC_5H_4)(PTA)] (0, 1, 3, 5, 7, 10 and 15 µM) at 24 (squares) or 72 h (circles).

Cell death studies. Previous studies on the alkynyl gold(I) derivative [Au(C≡CPh)(PTA)] revealed strong induction of intrinsic apoptosis on undifferentiated Caco-2/TC7 cells [20]. In consequence, we firstly assumed related cell death by apoptosis and performed flow cytometry analysis of annexin V/propidium iodide-stained Caco-2/TC7 cells.

After 24 h incubation with [Au(C≡C-2-NC_5H_4)(PTA)] we only observed a slight increase in late apoptotic levels (among 1.7-fold) (Table 3). These analyses also revealed a decrease in cell number after treatment with our gold compound (between two and three times), confirmed by Trypan blue exclusion test (Supplementary Material, Table T1).

Table 3. Percentages of Caco-2/TC7 cells undergoing cell death analyzed with double stain Annexin V and propidium iodide.

Treatment	Total events	Alive (%)	Necrosis (%)	Early apoptosis (%)	Late apoptosis (%)
Mock-treated	2408	75.6	0.9	15.3	8.2
[Au(C≡C-2-NC_5H_4)(PTA)]	1456	62.3	0.5	22.9	14.3

Then we investigated two common apoptotic features: cell cycle arrest [48] (Figure 3.1) and caspases 3 and 7 activation [18] (Figure 3.2). No significant differences were observed in comparison with mock-treated cells in both cases. Moreover, nuclear staining with Hoechst 33342 revealed changes in nuclear morphology after treatment with [Au(C≡C-2-NC_5H_4)(PTA)] (Figure 3.2), showing a clear swelling that is not a typical apoptotic feature [18,19]. The absence of apoptotic biomarkers in addition to the statements of Pietkiewicz *et al* [49] -it is impossible to distinguish between late apoptotic and necroptotic cells by using the classical double staining annexin V-PI- were evidences of a different type of cell death induction than apoptosis. Thus, we investigated necroptosis induction.

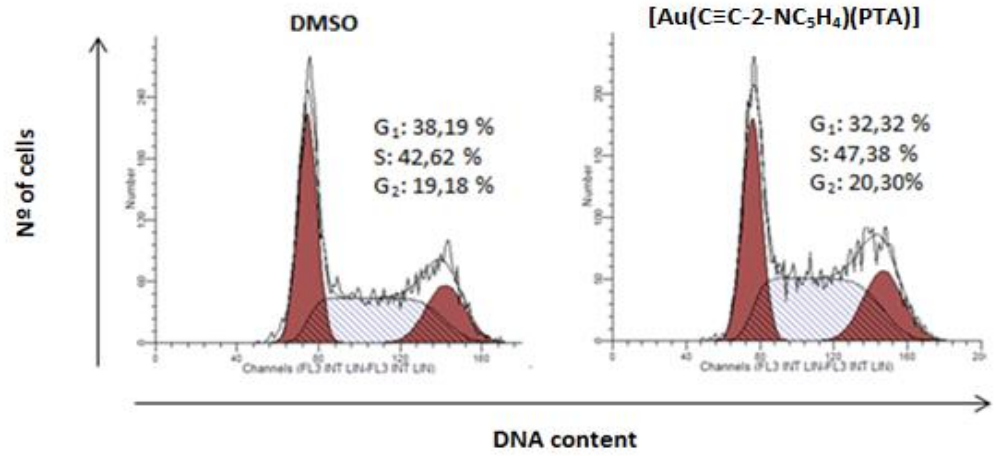

Figure 3.1 Cell cycle analysis. Percentages of cells undergoing each phase are showed.

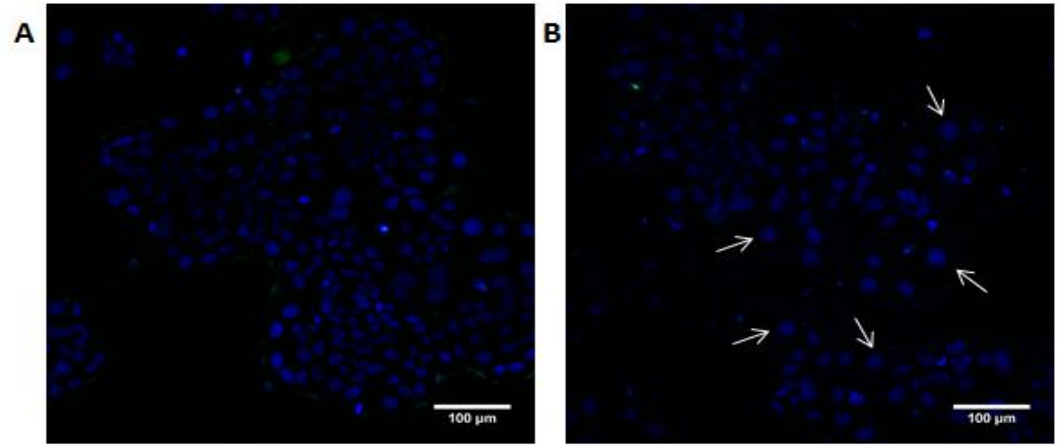

Figure 3.2 Double staining with Hoechst 33342 and *CellEvent Caspase-3/7 Green detection reagent* after 24 h treatment with A) DMSO or B) [Au(C≡C-2-NC5H4)(PTA)], (3.8 µM). Nuclei swelling are also highlighted (white arrows).

[Au(C≡C-2-NC_5H_4)(PTA)] does not bind DNA. We evaluated the possible interaction of this alkynyl derivative with DNA by monitoring its influence on pIRES2-EGFP (5308 pb) plasmid DNA by agarose gel electrophoresis in comparison to *cisplatin*. Figure S10 displays that mobility of the plasmid is not affected after incubation with increasing amounts of our gold derivative, unlike the variation observed with the reference drug. This lack of DNA interaction is shared with auranofin and other gold(I) derivatives [20,50].

[Au(C≡C-2-NC_5H_4)(PTA)] triggers necroptosis via ROS generation. The best characterized form of necroptosis is the one triggered by the cytokine Tumor Necrosis Factor-alpha (TNF-α). In TNF-α-triggered necroptosis, TNF receptor 1 (TNFR1) is stimulated by TNF binding and, as a consequence of its activation, recruits different proteins including RIP-1 in order to form a transient protein complex. Once in this complex, RIP-1 is ubiquitinated, necessary for NF-κB activation and the final consecution of necroptosis [51]. Given the importance of these three proteins for necroptosis induction, we investigated the effect of their inhibition on [Au(C≡C-2-NC_5H_4)(PTA)]-triggered cell death. Co-incubation of Caco-2 cells with our gold complex and the RIP-1 inhibitor necrostatin-1 (Nec-1) (50 μM, 1 h pre-incubation; Figure 4.A), a TNFR1 analog (2 μM, 1 h pre-incubation; Figure 5A) and the NF-κB inhibitor SN50 (1 μM, 1 h pre-incubation; Figure 5B) conducted to an increased survival ratio. Moreover, flow cytometry analysis revealed an increase of 8.5-fold in RIP-1 expression levels after incubation with [Au(C≡C-2-NC_5H_4)(PTA)] (Figure 4B), which confirms the role of this protein in cell death.

Further flow cytometry cell death studies revealed that co-incubation of our gold complex and Nec-1 resulted in a decrease of cells undergoing late apoptosis in addition of an increase in early apoptotic cells (Supplementaty Material Figure S11). This result indicates that necroptosis disruption might favor apoptotic cell death.

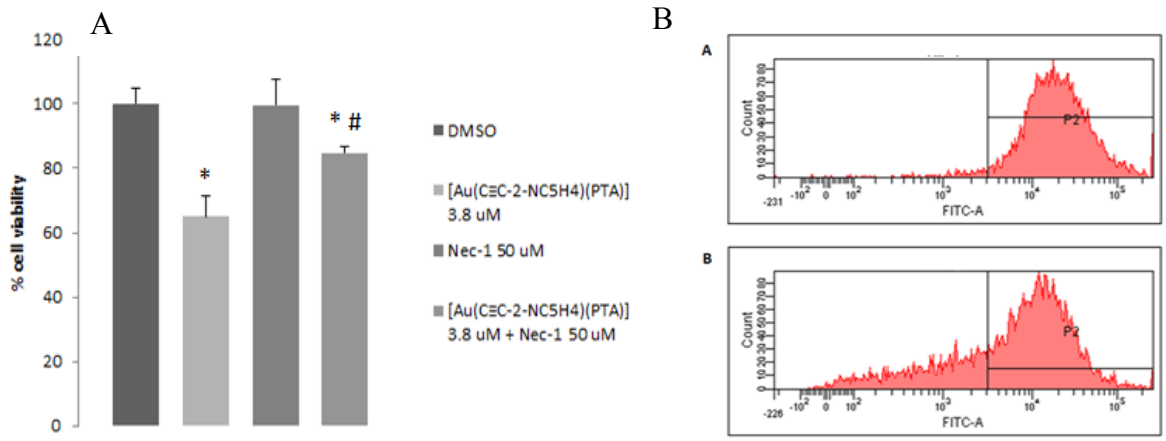

Figure 4. A) Effect of Nec-1 (50 μM, 1h) against [Au(C≡C-2-NC_5H_4)(PTA)] (3.8 μM). *p<0.05 respect to mock-treated cells. #p<0.05 respect to treatment with [Au(C≡C-2-NC_5H_4)(PTA)] (3.8 μM). B) RIP-1 expression levels after 24 h treatment with DMSO (panel A) or [Au(C≡C-2-NC_5H_4)(PTA)] (3.8 μM). (panel B).

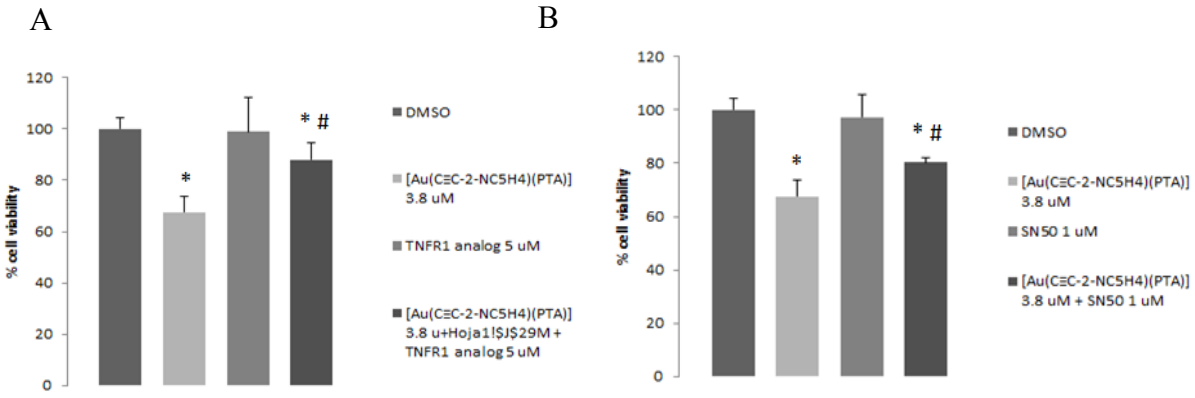

Figure 5. A) Effect of TNFR1 analog (5 μM, 1 h) against [Au(C≡C-2-NC_5H_4)(PTA)] (3.8 μM). *p<0.05 respect to mock-treated cells. #p<0.05 respect to treatment with [Au(C≡C-2-NC_5H_4)(PTA)] (3.8 μM). B) Effect of SN50 (1 μM, 1 h) against [Au(C≡C-2-NC_5H_4)(PTA)] (3.8 μM). *p<0.05 respect to mock-treated cells. #p<0.05 respect to treatment with [Au(C≡C-2-NC_5H_4)(PTA)] (3.8 μM).

The balanced character between lipophility and hydrophilicity of our gold complex allows its entrance in mitochondria. The luminescent properties of [Au(C≡C-2-NC_5H_4)(PTA)] [33] let us to perform co-localization studies using the mitochondrial dye *Mitotracker® Deep Red*. Microscopy fluorescence assay showed a high co-

localization between the gold complex and this organelle via the Van Steensel co-localization test (Figure 6.1). The accumulation of [Au(C≡C-2-NC_5H_4)(PTA)] in mitochondria disrupts its normal function, inducing a loss of mitochondrial membrane potential ($\Delta\psi_m$) as can be observed in Figure 6.2 As a result, an imbalance in normal ROS generation is produced. Total oxidative stress was investigated using the fluorogenic probe *CellROX® Deep Red Reagent*. The cell-permeant dye is non-fluorescent while in a reduced state, but exhibits bright fluorescence upon oxidation by ROS, so the fluorescence signal correlates with ROS levels. Fluorescence signal was significant higher after [Au(C≡C-2-NC_5H_4)(PTA)] treatment, revealing a great amount of oxidative stress induced (Figure 7.1). Since mitochondrial and extramitochondrial abnormal ROS generation has been related to necroptotic cell death without caspase activation [23] and some authors argue that RIP-1 might directly disrupt normal mitochondrial function and therefore contribute to the increase of ROS levels, [52] we measured H_2O_2 levels after [Au(C≡C-2-NC_5H_4)(PTA)] in presence or absence of Nec-1. Pre-incubation with Nec-1 resulted in no changes in H_2O_2 levels, similar to mock-treated cells or cells treated with the ROS inhibitor N-acetyl-cysteine (NAC) (Figure 7.2). Abnormally increased ROS levels are usually involved in apoptosis, high amounts of H_2O_2 have been found able to inhibit caspases and as a result trigger necrotic death [53, 54]. Furthermore, MTT assay revealed the protective effect of NAC against [Au(C≡C-2-NC_5H_4)(PTA)] (Figure S12), which finally probed the role of ROS in cell death.

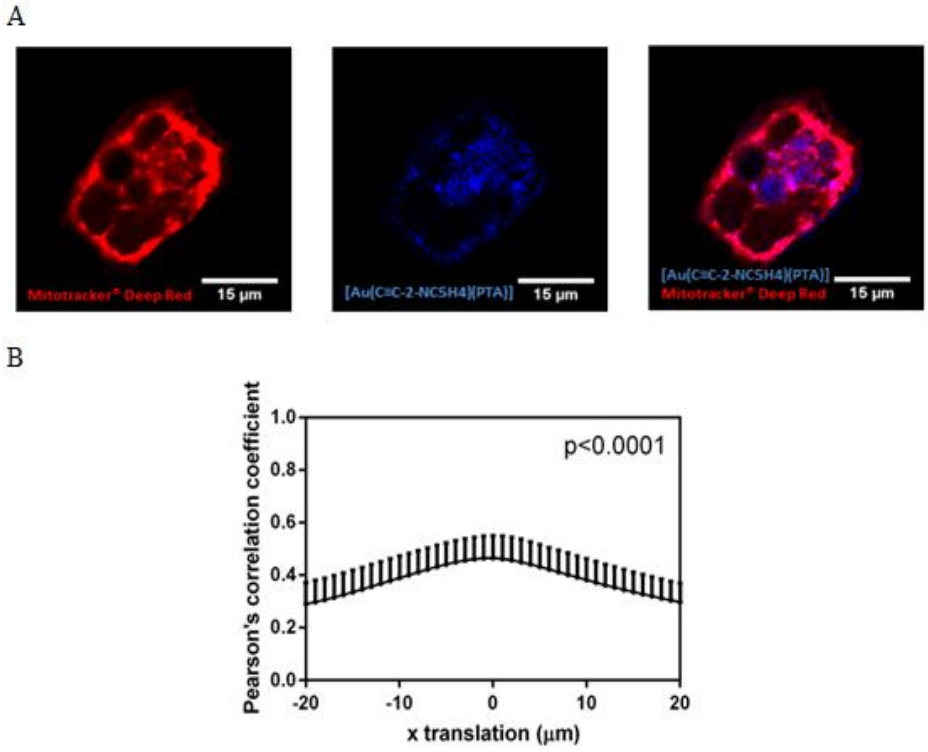

Figure 6.1 A) Co-localization of [Au(C≡C-2-NC_5H_4)(PTA)] 3.8 µM and mitochondria after 24 h incubation. B) Co-localization graph of [Au(C≡C-2-NC_5H_4)(PTA)] and mitochondria as determined via Van Steensel co-localization test of the images show in A.

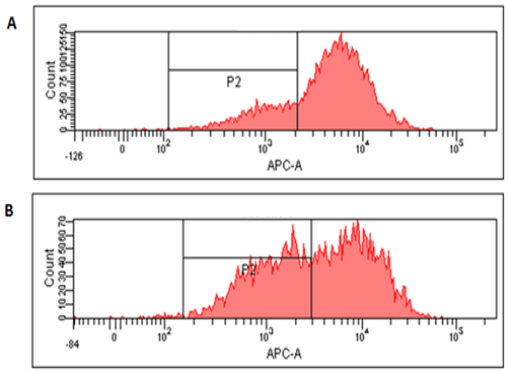

Figure 6.2 Representative histograms of effects on mitochondrial membrane potential after 24 h treatment with DMSO (panel A) or [Au(C≡C-2-NC_5H_4)(PTA)] (10 µM) (B).

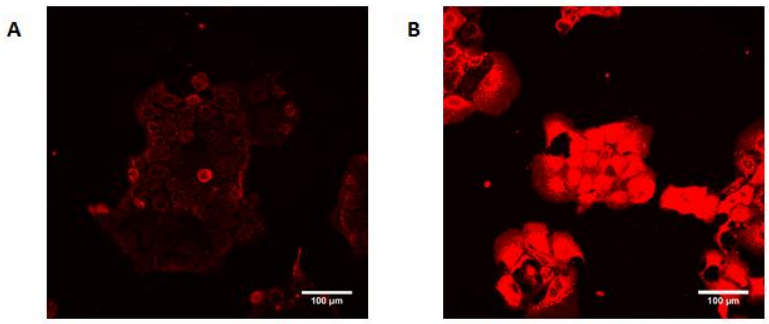

Figure 7.1 ROS generation after incubation with A) DMSO or B) [Au(C≡C-2-NC_5H_4)(PTA)] (3.8 µM) for 80 min.

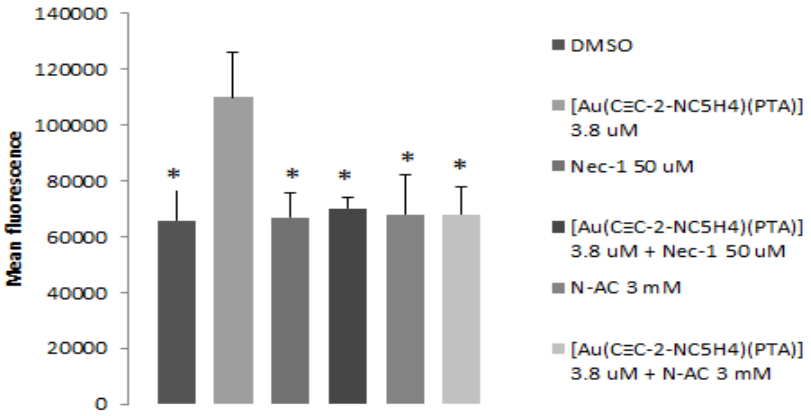

Figure 7.2 H_2O_2 generation after incubation with [Au(C≡C-2-NC_5H_4)(PTA)] (3.8 µM) for 80 min with or without pre-incubation with Nec-1 (50 µM, 1h) or NAC (3 mM, 1h). *p<0.05 respect to treatment with [Au(C≡C-2-NC_5H_4)(PTA)] (3.8 µM).

[Au(C≡C-2-NC_5H_4)(PTA)] shows how small changes in structure lead to different properties and behavior against cancerous cells. Thus, this complex links BSA much stronger than the related [Au(C≡C-C_6H_5)(PTA)] ($K_b = 2.46 \cdot 10^8$ *vs* $7.2 \cdot 10^4$ M^{-1}) [20] and induces necroptotic cell death in CRC cells with an increase in ROS production and a minimal inhibition of TrxR and without effect on glutathione reductase activity (Supplementary Material, Table T2 and T3). However, the counterpart [Au(C≡C-C_6H_5)(PTA)] triggers mitochondrial apoptotic by inhibiting TrxR and consequently increasing ROS levels. The main difference between both derivatives resides on the heteroatom N in the alkynyl unit. This pyridyl unit could favor additional interactions between neighboring molecules, as has been observed previously in the analogous 4-pyridylethynyl derivative with PTA [55]. The reported complex, which unlike our

derivative is very soluble in water, shows the formation of gel structure in water solution, giving rise to long fibers, thanks to π- π interactions between the pyridyl units. The occurrence of similar π- π interactions in our complex between the PTA molecule and the pyridyl unit is less probable, since any trace data could be retrieved from the corresponding 2D-NOESY spectrum, (Figure S9). Nevertheless, the position of the N atom in the pyridyl ring could support additional N-metal interactions between two molecules besides metal-triple bond contacts, as occurred in [Au(C≡C-2-NC_5H_4)(PPh_3)] [56].

Effect of [Au(C≡C-2-NC_5H_4)(PTA)] on Caco-2 spheroids (3D model). We tested increasing concentrations of [Au(C≡C-2-NC_5H_4)(PTA)] on Caco-2 spheroids. The morphology of spheroids may vary attending to different factors which include the inherent nature of cells or cell culture conditions. According to Nath *et al* [28], Caco-2 spheroids showed a "grape-like" morphology.

We studied cell viability by means of a double staining Hoechst 33342(blue)-PI(red) and fluorescence microscopy. The increase in red fluorescence in response to gold complex concentrations (Figure 8) correlated with a gradual decrease in survival ratio, since PI only stains dead cells. In addition, nuclei swelling indicated with white arrows is consistent with cells undergoing necroptotic cell death, as mentioned in Figure 3.2.

Viability studies revealed that our gold compound induced cell death in a tumor-like environment (Figure 8), which suggests that its anticancer properties may remain unchanged into a living organism. It is remarkable that, although in 3D model the decrease in viability observed was lower than the found in 2D for the same gold complex concentrations, cell properties differ greatly between each experiment as has been widely discussed previously. Consequently, these results support our initial hypothesis that this gold(I) complex has a considerable antitumor potential and it is not ruled out its chemotherapeutic use in the future.

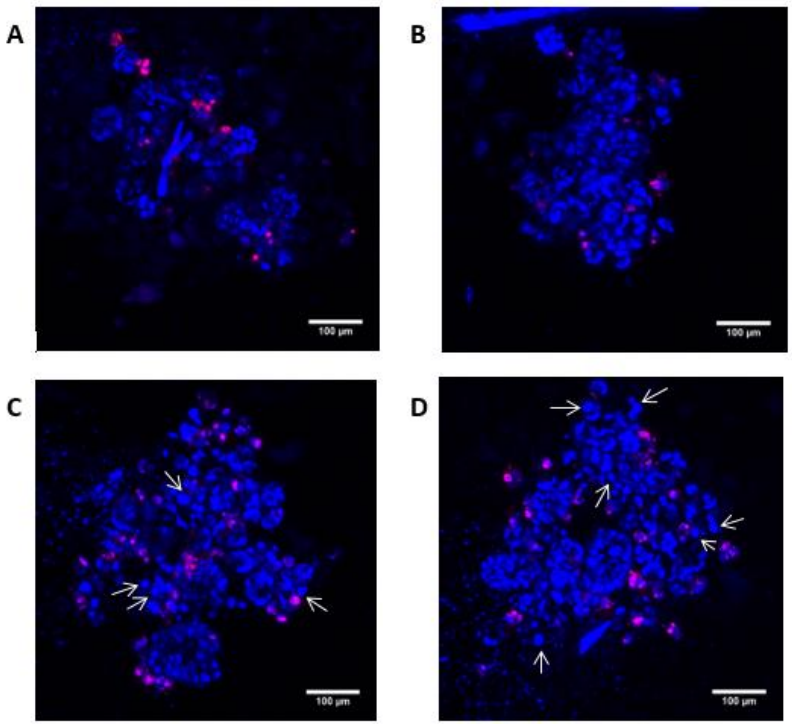

Figure 8. Fluorescence microscopy images of Caco-2 spheroids in response to 24 h incubation [Au(C≡C-2-NC_5H_4)(PTA)] A) 0 µM B) 3 µM C) 4µM and D) 5 µM. Nuclei swelling are also highlighted (white arrows).

CONCLUSSIONS

The antitumor potential of a previously characterized alkynyl gold(I) complex ([Au(C≡C-2-NC_5H_4)(PTA)]) has been evaluated on colorectal adenocarcinoma Caco-2 cell line. A strong interaction between a blood plasma protein (BSA) and the gold complex has been calculated, which makes the complex suitable for transportation by the protein through blood and release to the target and suitable for chemotherapy treatments. Its balanced character between lipophilicity and hydrophilicity allows it going across cell membranes. Therefore, ([Au(C≡C-2-NC_5H_4)(PTA)]) goes through mitochondrial membrane and alters its function, inducing an increase in ROS levels. The abnormal production of ROS triggers TNF-induced necroptosis dependent of RIP-1 activation and NF-κB signaling. Furthermore, we have proved that this compound maintains its therapeutic properties in a tumor-like environment using 3D model spheroids. In addition, we have demonstrated how small changes in the structure, namely an additional N atom in the alkyne skeleton, lead to different properties and behavior against cancerous cells. The findings of the present work provide a new insight into the use of gold as a substitute for platinum in chemotherapy, since [Au(C≡C-C_5H_4)(PTA)] has proved its efficacy against tumors at lower concentrations than cisplatin. Moreover, since its mechanism of action is via necroptosis, our complex could be used in the treatment of tumors resistant to apoptosis. To our knowledge, this is the first report of an alkynyl gold(I) complex able to induce necroptosis in cancer cells.

ABBREVIATIONS

TrxR: thioredoxin reductase, ROS: Reactive oxygen species, CRC: colorectal cancer, RIP-1: receptor-interacting protein 1, MLKL: mixed lineage kinase domain-like, TNF: tumor necrosis factor, DMEM: Dulbecco's modified Eagles medium, FBS: fetal bovine serum, MTT: 3-(4,5-dimethyl-2-thiazoyl)-2,5-diphenyltetrazolium bromide, DMSO: dimethyl sulfoxide, PI: propidium iodide, DCF: dichlorofluorescein, DilC1: 1,1',3,3,3'-

hexamethylindodicarbo-cyanine iodide, DTNB: 5,5-dithio-bis-(2-nitrobenzoic acid), PS: phosphatidylserine, Nec-1: necrostatin-1

NAC: N-acetyl-cysteine, $\Delta\psi_m$: mitochondrial membrane potential

ASSOCIATED CONTENT

Supporting Information. Supplementary data to this article can be found online

Corresponding Author

Elena Cerrada: ecerrada@unizar.es and Mª Jesús Rodrigez Yoldi: mjrodyol@unizar.es

Author Contributions

IM, EC and MJRY were responsible for the overall direction of the research. EC performed the synthesis of the gold compound and studied BSA interaction and solution chemistry. IM performed cell culture experiments supervised by MJRY. MVM and IM performed fluorescence microscopy experiments. IM, JQ and CSdD analyzed the data. The manuscript was written through contributions of all authors. All authors have given approval to the final version of the manuscript.

ACKNOWLEDGMENT

We thank Sonia Gascón for her technical assistance. We thank The Ministerio de Economia y Competitividad (CTQ2016-75816-C2-1-P and SAF2016-75441-R) and DGA (A-32 and E104) for financial support. MVM acknowledges the Ministerio de Educación, Cultura y Deportes of the Spanish Government for financial support.

REFERENCES

1. Muhammad, N., and Guo, Z. Metal-based anticancer chemotherapeutic agents, Curr. Opin. Chem. Biol. 19 (2014) 144-153.
2. Komeda, S., and Casini, A. Next-generation anticancer metallodrugs, Curr. Top. Med. Chem. 12 (2012) 219-235.
3. Karasawa, T., and Steyger, P. S. An integrated view of cisplatin-induced nephrotoxicity and ototoxicity, Toxicol. Lett. 237 (2015) 219-227.
4. Garcia-Moreno, E., Tomas, A., Atrian-Blasco, E., Gascon, S., Romanos, E., Rodriguez-Yoldi, M. J., Cerrada, E., and Laguna, M. *In vitro* and *in vivo* evaluation of organometallic gold(I) derivatives as anticancer agents, Dalton Trans. 45, (2016) 2462-2475.

5. Lammer, A. D., Cook, M. E., and Sessler, J. L. Synthesis and anti-cancer activities of a water soluble gold(III) porphyrin, J. Porphyr. Phthalocyanines 19 (2015) 398-403.
6. Yang, M., Pickard, A. J., Qiao, X., Gueble, M. J., Day, C. S., Kucera, G. L., and Bierbach, U. Synthesis, reactivity, and biological activity of Gold (I) complexes modified with thiourea-functionalized tyrosine kinase inhibitors, Inorg. Chem. 54 (2015) 3316-3324.
7. Garcia-Moreno, E., Gascon, S., A Garcia de Jalon, J., Romanos, E., Jesus Rodriguez-Yoldi, M., Cerrada, E., and Laguna, M. *In Vivo* Anticancer Activity, Toxicology and Histopathological Studies of the Thiolate Gold (I) Complex [Au (Spyrimidine)(PTA-CH2Ph)] Br, Anticancer Agents Med. Chem. 15 (2015) 773-782.
8. Zou, T., Lum, C. T., Lok, C. N., To, W. P., Low, K. H., and Che, C. M. A binuclear gold(I) complex with mixed bridging diphosphine and bis(N-heterocyclic carbene) ligands shows favorable thiol reactivity and inhibits tumor growth and angiogenesis *in vivo*, Angew Chem. Int. Ed. Engl. 53 (2014) 5810-5814.
9. Bazzicalupi, C., Ferraroni, M., Papi, F., Massai, L., Bertrand, B., Messori, L., Gratteri, P., Casini, A. Determinants for tight and selective binding of a medicinal dicarbene gold(I) complex to a telomeric DNA g-quadruplex: a joint ESI MS and XRD investigation. Angew. Chem. Int. Ed. Engl. 55 (2016) 4256-9
10. Bertrand, B., Stefan, L., Pirrotta, M., Monchaud, D., Bodio, E., Richard, P., Le Gendre, P., Warmerdam, E., de Jager, M.H., Groothuis, G.M., Picquet, M., Casini, A. Caffeine-based gold(I) N-heterocyclic carbenes as possible anticancer agents: synthesis and biological properties. Inorg. Chem. 53 (2014) 2296-303
11. Mendes, F., Groessl, M., Nazarov, A.A., Tsybin, Y.O., Sava, G., Santos, I., Dyson, P.J., Casini, A. Metal-based inhibition of poly(ADP-ribose) polymerase—the guardian angel of DNA. J. Med. Chem. 54 (2011) 2196-206
12. Ortego, L., Cardoso, F., Martins, S., Fillat, M. F., Laguna, A., Meireles, M., Villacampa, M. D., and Gimeno, M. C. Strong inhibition of thioredoxin reductase by highly cytotoxic gold (I) complexes. DNA binding studies, J. Inorg. Biochem. 130 (2014) 32-37.
13. Mahmood, D. F., Abderrazak, A., El Hadri, K., Simmet, T., and Rouis, M. The thioredoxin system as a therapeutic target in human health and disease, Antioxid. Redox Signal 19 (2013) 1266-1303.
14. Marzano, C., Gandin, V., Folda, A., Scutari, G., Bindoli, A., and Rigobello, M. P. Inhibition of thioredoxin reductase by auranofin induces apoptosis in cisplatin-resistant human ovarian cancer cells, Free Radic. Biol. Med. 42 (2007) 872-881.
15. Mármol, I., Sánchez-de-Diego, C., Pradilla Dieste, A., Cerrada, E., and Rodriguez Yoldi, M. J. Colorectal carcinoma: a general overview and future perspectives in colorectal cancer, Int. J. Mol. Sci. 18 (2017) 197.
16. de Gramont, A., Figer, A., Seymour, M., Homerin, M., Hmissi, A., Cassidy, J., Boni, C., Cortes-Funes, H., Cervantes, A., Freyer, G., Papamichael, D., Le Bail, N., Louvet, C., Hendler, D., de Braud, F., Wilson, C., Morvan, F., and Bonetti, A. Leucovorin and fluorouracil with or without oxaliplatin as first-line treatment in advanced colorectal cancer, J. Clin. Oncol. 18 (2000) 2938-2947.
17. Rothenberg, M. L. Efficacy of oxaliplatin in the treatment of colorectal cancer, Oncology (Williston Park) 14 (2000) 9-14.

18. Chaabane, W., User, S. D., El-Gazzah, M., Jaksik, R., Sajjadi, E., Rzeszowska-Wolny, J., and Łos, M. J. Autophagy, apoptosis, mitoptosis and necrosis: interdependence between those pathways and effects on cancer, Arch. Immunol. Ther. Exp. (Warsz) 61 (2013) 43-58.
19. Green, D. R., and Llambi, F. Cell Death Signaling, Cold Spring Harb. Perspect. Biol. 7 (2015) a006080.
20. Sanchez-de-Diego, C., Marmol, I., Perez, R., Gascon, S., Rodriguez-Yoldi, M. J., and Cerrada, E. The anticancer effect related to disturbances in redox balance on Caco-2 cells caused by an alkynyl gold(I) complex, J. Inorg. Biochem. 166 (2017) 108-121.
21. Fulda, S. Tumor resistance to apoptosis, Int. J. Cancer. 124 (2009) 511-5
22. He, S., Huang, S., and Shen, Z. Biomarkers for the detection of necroptosis, Cell. Mol. Life Sci. 73 (2016) 2177-2181.
23. Chen, D., Yu, J., and Zhang, L. Necroptosis: an alternative cell death program defending against cancer, Biochim. Biophys. Acta 1865 (2016) 228-236.
24. Ravi, M., Paramesh, V., Kaviya, S. R., Anuradha, E., and Solomon, F. D. 3D cell culture systems: advantages and applications, J. Cell. Physiol. 230 (2015) 16-26.
25. Thoma, C. R., Zimmermann, M., Agarkova, I., Kelm, J. M., and Krek, W. 3D cell culture systems modeling tumor growth determinants in cancer target discovery, Adv. Drug Deliv. Rev. 69-70 (2014) 29-41.
26. Edmondson, R., Broglie, J. J., Adcock, A. F., and Yang, L. Three-Dimensional Cell Culture Systems and Their Applications in Drug Discovery and Cell-Based Biosensors, Assay Drug Dev. Technol. 12 (2014) 207-218.
27. Xu, X., Farach-Carson, M. C., and Jia, X. Three-Dimensional In Vitro Tumor Models for Cancer Research and Drug Evaluation, Biotechnol. Adv. 32 (2014) 1256-1268.
28. Nath, S., and Devi, G. R. Three-dimensional culture systems in cancer research: Focus on tumor spheroid model, Pharmacol. Ther. 163 (2016) 94-108.
29. Theodoraki, M. A., Rezende, C. O., Jr., Chantarasriwong, O., Corben, A. D., Theodorakis, E. A., and Alpaugh, M. L. Spontaneously-forming spheroids as an in vitro cancer cell model for anticancer drug screening, Oncotarget 6 (2015) 21255-21267.
30. Ham, S. L., Joshi, R., Luker, G. D., and Tavana, H. Engineered Breast Cancer Cell Spheroids Reproduce Biologic Properties of Solid Tumors, Adv. Healthc. Mater 5 (2016) 2788-2798.
31. Lee, J. B., Son, S. H., Park, M. C., Kim, T. H., Kim, M. G., Yoo, S. D., and Kim, S. A novel *in vitro* permeability assay using three-dimensional cell culture system, J. Biotechnol. 205 (2015) 93-100.
32. Zeller, P., Bricks, T., Vidal, G., Jacques, S., Anton, P. M., and Leclerc, E. Multiparametric temporal analysis of the Caco-2/TC7 demonstrated functional and differentiated monolayers as early as 14 days of culture, Eur. J. Pharm. Sci. 72 (2015) 1-11.
33. Vergara, E., Cerrada, E., Casini, A., Zava, O., Laguna, M., and Dyson, P. J. Antiproliferative activity of gold (I) alkyne complexes containing water-soluble phosphane ligands, Organometallics 29 (2010) 2596-2603.
34. van Meerloo, J., Kaspers, G. J., and Cloos, J. Cell sensitivity assays: the MTT assay, Methods Mol. Biol. 731 (2011) 237-245.

35. Ruiz-Leal, M., and George, S. An *in vitro* procedure for evaluation of early stage oxidative stress in an established fish cell line applied to investigation of PHAH and pesticide toxicity, Mar Environ. Res. 58 (2004) 631-635.
36. Ayuso, J. M., Basheer, H. A., Monge, R., Sanchez-Alvarez, P., Doblare, M., Shnyder, S. D., Vinader, V., Afarinkia, K., Fernandez, L. J., and Ochoa, I. Study of the Chemotactic Response of Multicellular Spheroids in a Microfluidic Device, PLoS One 10 (2015) e0139515.

37. Lombardo, F., Obach, R. S., Shalaeva, M. Y., and Gao, F. Prediction of volume of distribution values in humans for neutral and basic drugs using physicochemical measurements and plasma protein binding data, J. Med. Chem. 45 (2002) 2867-2876.

38. Fonteh, P., Elkhadir, A., Omondi, B., Guzei, I., Darkwa, J., and Meyer, D. Impedance technology reveals correlations between cytotoxicity and lipophilicity of mono and bimetallic phosphine complexes, Biometals 28 (2015) 653-667.
39. Liu, J. J., Galettis, P., Farr, A., Maharaj, L., Samarasinha, H., McGechan, A. C., Baguley, B. C., Bowen, R. J., Berners-Price, S. J., and McKeage, M. J. *In vitro* antitumour and hepatotoxicity profiles of Au(I) and Ag(I) bidentate pyridyl phosphine complexes and relationships to cellular uptake, J. Inorg. Biochem. 102 (2008) 303-310.
40. Berners-Price, S. J., and Filipovska, A. The design of gold-based, mitochondria-targeted chemotherapeutics, Australian J Chem. 61 (2008) 661-668.
41. Finlay, G. J., and Baguley, B. C. Effects of protein binding on the *in vitro* activity of antitumour acridine derivatives and related anticancer drugs, Cancer Chemother. Pharmacol. 45 (2000) 417-422.
42. He, X. M., and Carter, D. C. Atomic structure and chemistry of human serum albumin, Nature 358 (1992) 209-215.
43. Yamasaki, K., Maruyama, T., Kragh-Hansen, U., and Otagiri, M. Characterization of site I on human serum albumin: concept about the structure of a drug binding site, Biochim. Biophys. Acta 1295 (1996) 147-157.
44. Eftink, M. R., and Ghiron, C. A. Fluorescence quenching studies with proteins, Anal. Biochem. 114 (1981) 199-227.
45. Ross, P. D., and Subramanian, S. Thermodynamics of protein association reactions: forces contributing to stability, Biochemistry 20 (1981) 3096-3102.
46. Veeralakshmi, S., Nehru, S., Arunachalam, S., Kumar, P., Govindaraju, M. Study of single and double chain surfactant-cobalt(III) complexes and their hydrophobicity, micelle formation, interaction with serum albumins and antibacterial activities. Inorg. Chem. Front. 1 (2014) 393-404
47. Atrián-Blasco, E., Gascón, S., Rodríguez-Yoldi, M.J., Laguna, M., Cerrada, E. Synthesis of gold(I) derivatives bearing alkylated 1,3,5,-triaza-7-phosphaadamantane as selective anticancer metallodrugs. Eur. J. Inorg. Chem. 17 (2016) 2891-2803
48. Clarke, P. R., and Allan, L. A. Cell-cycle control in the face of damage--a matter of life or death, Trends Cell. Biol. 19 (2009) 89-98.
49. Pietkiewicz, S., Schmidt, J. H., and Lavrik, I. N. Quantification of apoptosis and necroptosis at the single cell level by a combination of Imaging Flow Cytometry

with classical Annexin V/propidium iodide staining, J. Immunol. Methods 423 (2015) 99-103.
50. Mirabelli, C. K., Sung, C. M., Zimmerman, J. P., Hill, D. T., Mong, S., and Crooke, S. T. Interactions of gold coordination complexes with DNA, Biochem. Pharmacol. 35 (1986) 1427-1433.
51. Liu, X., Shi, F., Li, Y., Yu, X., Peng, S., Li, W., Luo, X., and Cao, Y. Post-translational modifications as key regulators of TNF-induced necroptosis, Cell. Death Dis. 7 (2016) e2293.
52. Ye, Y. C., Wang, H. J., Yu, L., Tashiro, S., Onodera, S., and Ikejima, T. RIP1-mediated mitochondrial dysfunction and ROS production contributed to tumor necrosis factor alpha-induced L929 cell necroptosis and autophagy, Int. Immunopharmacol. 14 (2012) 674-682.
53. Borutaite, V., and Brown, G. C. Caspases are reversibly inactivated by hydrogen peroxide, FEBS Letters 500 (2001) 114-118.
54. Saito, Y., Nishio, K., Ogawa, Y., Kimata, J., Kinumi, T., Yoshida, Y., Noguchi, N., and Niki, E. Turning point in apoptosis/necrosis induced by hydrogen peroxide, Free Radic. Res. 40 (2006) 619-630.
55. Gavara, R., Llorca, J., Lima, J. C., and Rodriguez, L. A luminescent hydrogel based on a new Au(I) complex, Chem. Commun. (Camb) 49 (2013) 72-74.
56. Blanco, M. C., Cámara, J., Gimeno, M. C., Jones, P. G., Laguna, A., López-de-Luzuriaga, J. M., Olmos, M. E., and Villacampa, M. D. Luminescent homo-and heteropolynuclear gold complexes stabilized by a unique acetylide fragment, Organometallics 31 (2011) 2597-2605.

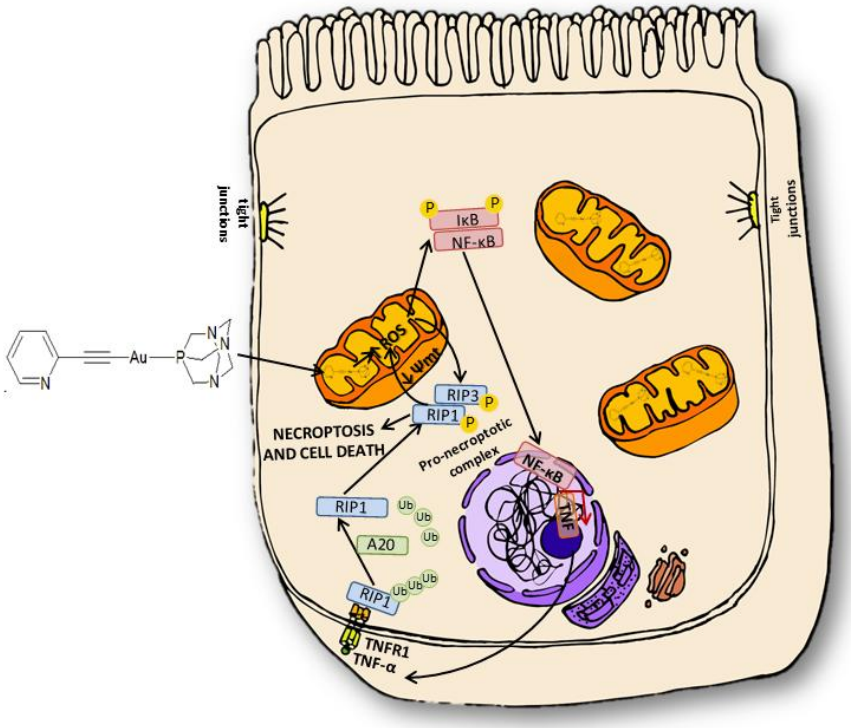

Graphical abstract

HIGHLIGHTS

- Gold(I) complex [Au(C≡C-2-NC_5H_4)(PTA)] induces necroptosis on Caco-2 cells.
- The complex enters the mitochondria, alters its function and produces ROS increase.
- Necroptosis depends on ROS increase, TNF-α, RIP-1 activation and NF-κB signaling.
- [Au(C≡C-2-NC_5H_4)(PTA)] induces cell death on 2D and 3D colorectal carcinoma model
- This is the first evidence of gold compound able to overcome apoptosis resistance.